 FDMP, vol.5, no.1, pp.93-121, 2009

Prediction of Erosion Wear in Multi-Size Particulate Flow through a Rotating Channel

K.V. Pagalthivarthi[1] and P.K. Gupta[2]

Abstract: The objective of the present work is to predict erosive wear in multi-size dense slurry flow in a rotating channel. The methodology comprises numerical prediction of two-phase flow which is accomplished using the Galerkin finite element method. The wear models for both sliding wear and impact wear mechanisms account for the particle size dependence. The effect of various operating parameters such as rotation rate, solids concentration, flow rate, particle size distribution and so forth has been studied. Results indicate that wear rate in general increases along the pressure-side of the channel with rotation rate, overall solids concentration, flow rates etc. The wear models in the present study are able to capture the particle size distribution fairly well. It is concluded that accurate wear prediction could be obtained by characterizing the particle size distribution into suitable number of size classes, and accounting for the particle-size dependence in the wear model(s).

Keywords: Dense slurry, particle size distribution, rotating channel, sliding wear rate, impact wear rate.

1 Introduction

Particulate flow induced erosion is a major cause of concern in several applications such as mining, metallurgical, dredging, power and propulsion industries, where solid-gas and/or solid-liquid (slurries) mixtures are transported through rotating passages. For example, the presence of particles in wetted components of the centrifugal slurry pump such as the impeller affects not only the erosion life of its components but also its hydraulic performance. The extent of damage due to erosion could be so severe that sometimes it is seen to hole through the component. Due to such detrimental effects, not only the useful life of the component is reduced, but also the ownership cost escalates due to the unscheduled shutdown (downtime)

[1] CFD Research Leader, GIW Industries Inc., Grovetown, GA - 30813, USA
[2] Asst. Prof., Dept. of Mech. Engg., SISTec, Bhopal, MP, India – 462036 (Corresponding Author)

of entire slurry pipeline system for replacing/repairing individual component parts. For example, it has been reported [Addie, Sellgren, Mudge (2001)] that an unscheduled downtime can cost in excess of 100,000 US$ per hour for a SAG mill slurry pump operating under the most severe of wear conditions. Therefore, from the viewpoints of hydrodynamical performance, useful life of pump components, cost of repairing/replacing worn out parts and the associated unscheduled downtime, erosive wear prediction has attracted considerable interest and concern over the years.

The erosion wear of the impeller has greater influence on the pump performance compared to other wet-end components. Apart from wear, presence of solids also reduces the head and efficiency. For example [Addie and Sellgren (1998)], in a water test carried out with a worn impeller that was about to fall apart, the pump head was reduced by 30% while the efficiency reduced by approximately 15%. The peripheral speed of an impeller that relates directly to the head produced is a key parameter affecting wear. This peripheral speed is related to both the impeller rotating speed and its diameter. In order to maintain a required head, pump rotating speed has to be increased. Generally, wear rate increases with increase in required rotary speed [Addie and Sellgren (1998)]. It is therefore deemed necessary to investigate the effect of various operating parameters such as the flow rate, rotation rate, inlet solids concentration and so forth on erosion wear.

The mechanism of wear in the slurry pump components [Roco, Nair, Addie (1984); Roco, Nair, Addie, Dennis (1984); Roco and Cader (1988); Addie and Pagalthivarthi (1989)] is attributed due to particle impact and/or sliding abrasive action (or scouring) of the solid particles as they move parallel to the surface. Particle impact could also be directional or random (due to turbulence). For dense slurry flows, the predominant mechanism of wear is due to sliding action of the solids [Tian, Addie, Pagalthivarthi (2005)]. Due to rotation, the Coriolis force presses the solid particles against the surface as the solids move across the channel [see Fig. 1]. As rotation increases, the solid particles form a sliding bed adjacent to the surface, minimizing particle impact.

Total wear depend on the local concentration of particles, particle velocity, shear stress and the material properties of both the particle and the wear surface. The local conditions of particulate velocity and concentration vary from point to point, and hence the wear rate also varies from point to point. An important consideration in the design process is to obtain nearly uniform wear rate over the whole surface so that there are no undesirable premature local failures due to erosion.

A numerically predictive tool for particulate flow enables the determination of particle concentration and velocity near the wear surface. As there is no universal theory that relates the solid-liquid flow conditions to the wear rate, a certain degree

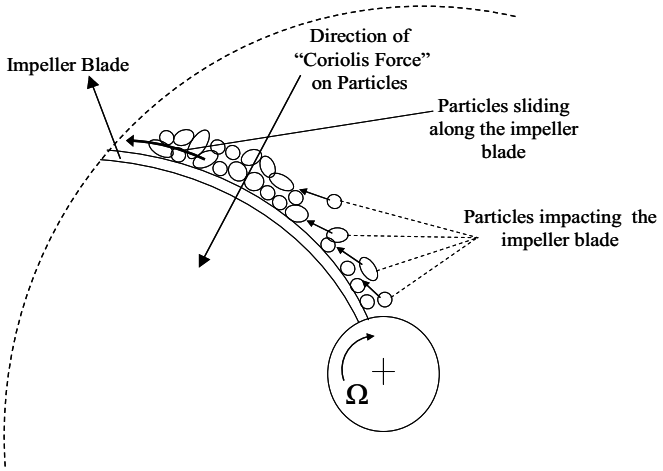

Figure 1: Schematic of impact and sliding wear in centrifugal pump impeller

of empiricism is unavoidable in the wear rate computation. Empirically determined wear coefficients are used to relate the flow conditions to the wear rate. Basically, the wear coefficients quantitatively represent the amount of particulate energy required to remove a unit volume of material. Experimental procedures for measuring both impact and sliding wear coefficients are described elsewhere [Roco, Nair, Addie, Dennis (1984); Pagalthivarthi and Helmly (1992); Tuzson and Scheibe-Powell (1984)] in the literature.

Through various studies [Roco and Addie (1983); Roco, Addie, Visintainer, Ray (1986); Pagalthivarthi and Veeraraghavan(1998); Tuzson and Clark (1998)], it has been well recognized that the specific energy for wear due to impact or sliding depends on particle size [Pagalthivarthi and Veeraraghavan(1998); Pagalthivarthi and Addie (2001)], particle shape, particle size distribution, material properties, hardness and microstructure of eroding material [Tian, Addie, Pagalthivarthi (2005)] and so forth.

Particle sizes in industrial slurries vary considerably over 2-3 orders of magnitude. In order to account for the broad particle size distribution, particles are characterized into several size classes [Gupta and Pagalthivarthi (2007); Kaushal, Seshadri, Singh (2002); Kaushal and Tomito (2003); Ravichandra, Pagalthivarthi, Sanghi (2005)] each with its representative particle diameter and fraction of the overall solids concentration. It is expected that in multi-size particulate flow, each particle will have its own contribution to the overall wear rate. An additional objective of the present work has been to study the effect of particle size distribution (PSD) on

the erosion wear.

A two-dimensional straight rotating channel serves as a useful simplification [Gupta and Pagalthivarthi (2007)] in studying the underlying physics involved in dense two-phase flow in such impellers. Thus, the erosion prediction methodology comprises essentially of three steps [Tian, Addie, Pagalthivarthi (2005); Pagalthivarthi and Helmly (1992); Pagalthivarthi and Addie (2001)]: (1) computation of two-phase flow field, (2) relating the local flow velocity and concentration near the wear surface to the wear rate *via* a suitable wear model, and (3) empirical determination of wear coefficient relevant to the wear model.

Computation of two-phase (or multi-size) flow is a vital step towards determining the local flow conditions near the wear surface. Numerical simulation using finite element method has been used to compute the multi-size particulate flow field in a two-dimensional large aspect ratio duct rotating [Gupta and Pagalthivarthi (2007)] in an orthogonal mode. For a detailed modeling and flow analysis of multi-size particulate flow in rotating channels, please see [Gupta and Pagalthivarthi (2007)]. The channel is completely immersed in water. Once the flow field is determined, the local concentration and velocity are correlated *via* the wear models to predict wear rates. The wear models used in this study account for the broad particle size distribution and are discussed in the sequel.

2 Impact wear rate

For monosize slurries [Roco, Nair, Addie, Dennis (1984)], the wear rate is correlated to the kinetic energy flux of the particles as

$$\dot{W}_I = \frac{\rho_s C_s V_s^3}{E_I(\alpha)}, \tag{1}$$

where ρ_s is the solids density, C_s is particle concentration, V_s is particle impact velocity and $E_I(\alpha)$ is the impact wear coefficient as a function of the impact angle α. Note that $\rho_s C_s V_s$ is the mass flux and V_s^2 is the kinetic energy per unit mass of the particles.

For some materials, the exponent of the velocity V_s can be different from 3.0. The impact wear coefficient is measured in a test rig in which a wedge of specified angle is placed head-on in a stream of slurry of known concentration and velocity. The extent of wear may be measured by weight loss or by using a profilometer to measure the varying wear depth.

The impact wear coefficient strongly depends on the impact angle, α. From the experimental results of [Roco, Nair, Addie, Dennis (1984)], the impact wear coefficient $E_I(\alpha)$ (also known as the specific energy $\left(J/m^3\right)$ for impact wear) for

Ni-Hard (a white iron alloy) material may be expressed as

$$E_I(\alpha) = \frac{E_0}{\frac{4\alpha}{\pi}\left(1-\frac{\alpha}{\pi}\right)},\ (\alpha \text{ in radians}), \tag{2}$$

where E_0 is the coefficient of the wearing surface for a normal impact ($\alpha = \pi/2$). This formula is inaccurate for very small angles. Hence for $\alpha < 2^\circ$, the value of $E_I(\alpha)$ at 2° is taken. The specific equation for each particle/wear material combination must be determined empirically. For hard white iron materials, the form of Eq. 1 is retained. However, the coefficient E_0 depends on the slurry material and particle size. For a given slurry material, therefore, E_0 (and hence $E_I(\alpha)$) depends on the particle size.

For multi-size particle flow, the overall impact wear rate is likely to be influenced by all the representative particle sizes. Thus the total impact wear rate is given as [Ravichandra (2004)]

$$\dot{W}_I = \sum_{k=1}^{N} \frac{\rho_k C_k V_k^3}{E_{Ik}(\alpha_k)}, \tag{3}$$

where $\rho_{k,} C_k$ and V_k are the density, concentration and velocity of particle size class k, and $E_{Ik}(\alpha)$ is the specific energy coefficient for impact wear for the k^{th} species. The velocity V_k is given by

$$V_k = \sqrt{u_k^2 + v_k^2}, \tag{4}$$

where u_k and v_k are x- and y- components of particle velocity ,V_k, and the angle of impact, $\alpha_k = \tan^{-1}\left(\frac{|v_k|}{|u_k|}\right)$. Based on experiments [Visintainer, Pagalthivarthi, Tian (2005)], the particle size dependence of $E_I\left(J/m^3\right)$ may be written as

$$E_I\left(\alpha_k, d_{pk}\right) = C_{adj} E_I(\alpha_k), \tag{5}$$

where d_{pk} is the particle diameter of the k^{th} species; $E_I(\alpha_k)$ is the value for $d_{pk} = 160\mu$m particles, and C_{adj} is an adjustable factor given as

$$C_{adj} = A_{im}\left[1.65 d_{p_k} + C_{im}\right]^{n_{im}} + B_{im}, \tag{6}$$

with A_{im}, B_{im}, C_{im} and n_{im} being determined experimentally. For a specific Ni-Cr white iron alloy material and sand slurries, the recommended values are [Visintainer, Pagalthivarthi, Tian (2005)]

$$\begin{aligned} A_{im} &= 8.578 \times 10^{10}, \\ B_{im} &= 3.645 \times 10^{-2}, \\ C_{im} &= 490, \text{ and} \\ n_{im} &= -3.668. \end{aligned} \tag{7}$$

In Eq. 6, d_{pk} is in micrometers. Thus for the multi-size particulate slurry the total impact wear rate

$$\dot{W}_I = \sum_{k=1}^{N} \frac{\rho_k C_k V_k^3}{E_I\left(\alpha_k, d_{pk}\right)}. \tag{8}$$

Note that the calculations presented in this study are restricted to the specific material whose wear coefficient is defined by Eq. 5-7.

In a rotating channel the particle velocities are generally directed towards the pressure side of the channel. Thus, directional impact is likely to occur mainly on the pressure side wall of the channel. In the present study, therefore, directional impact wear on the channel suction side is assumed to be negligible.

3 Sliding wear rate

Sliding wear is related to the abrading action of solids against the wearing surface. The frictional power associated with the particles in such a sliding action is used to relate the sliding wear rate *via* the specific energy of sliding. The sliding wear rate is therefore expressed as the ratio of friction power, P_{SL}, to the specific energy of sliding, E_{SP} $\left(J/m^3\right)$, as

$$\dot{W}_{SL} = \frac{P_{SL}}{E_{SP}}. \tag{9}$$

The frictional power associated with sliding particles is given as

$$P_{SL} = \tau_S u_{St}, \tag{10}$$

where τ_S and u_{St} are, respectively, the solids shear stress and the solids tangential velocity. In practice, erosion occurs when this friction power exceeds a critical threshold value. Usually this threshold value is relatively small compared to E_{SP}, and hence it may be neglected.

For multi-size particulate flow, the sliding wear rate is computed as the summation of sliding wear rates due to each size class. Thus, the sliding wear rate for multi-size particulate flow is expressed as

$$\dot{W}_{SL} = \sum_{k=1}^{N} \frac{C_k \tau_k u_k}{E_{SP}}, \tag{11}$$

where τ_k, C_k and u_k are, respectively, the shear stress, concentration and the tangential velocity of particulate species 'k'. The wall shear stress τ_k, is computed as

$$\tau_k = \rho_k u_{\tau k}^2, \tag{12}$$

where $u_{\tau k}$ is the friction velocity which is computed using the wall functions and the known (already computed) velocity field.

The sliding wear rate in Eq. 11 is based on the assumption that E_{SP} is constant. However, some studies [Tian, Addie, Pagalthivarthi (2005); Pagalthivarthi and Veeraraghavan (1998)] have shown strong dependence of the specific energy of sliding, E_{SP}, on particle size. In the experimental work [Tian, Addie, Pagalthivarthi (2005)] on slurries with narrowly-, semi-narrowly- and broadly-banded particle sizes, an "effective particle size" instead of D50 particle size is recommended to better represent the actual abrasivity (erosive wear) of slurries, particularly those with broad particle size distribution. The Coriolis wear tester is used in the study [Tian, Addie, Pagalthivarthi (2005)] to simultaneously test four specimens of different (wear surface) material. The Coriolis wear tester [Pagalthivarthi and Helmly (1992); Tuzson and Scheibe-Powell (1984); Clark, Tuzson, Wong (2000)] has been widely used to determine the specific energy of sliding wear in dense slurry flows. The particle size-dependent specific energy for sliding $\left(J/m^3\right)$ is given as

$$E_{SP}\left(d_{p_k}\right) = 10^8 \left[A_{sl}\left\{d_{p_k} + C_{sl}\right\}^{n_{sl}} + B_{sl}\right], \tag{13}$$

where, A_{sl}, B_{sl}, C_{sl} and n_{sl} are empirically determined constants for a particular material (and d_{pk} is in microns). In the present study, these empirical constants are chosen (for a specific white iron alloy material) as

$$\begin{aligned} A_{sl} &= 4.236 \times 10^{14}, \\ B_{sl} &= 180, \\ C_{sl} &= 490, \text{ and} \\ n_{sl} &= -3.861. \end{aligned} \tag{14}$$

Thus the particle size-dependent sliding wear rate is given as

$$\dot{W}_{SL} = \sum_{k=1}^{N} \frac{C_k \tau_k u_k}{E_{SP}\left(d_{p_k}\right)}. \tag{15}$$

The total wear rate is given as the sum of $\dot{W}_I$ and $\dot{W}_{SL}$.

4 Applications of wear models to pipes

Experimental results on wear rates in rotating/stationary straight channel are not available in the open literature. For the related problem of multi-size particulate flow in pipes, [Ravichandra (2004)] presents comparison of predicted normalized wear rates with the experimental results of [Gupta, Singh, Seshadri (1995)].

This comparison is used as the basis of confidence in the present wear calculation methodology. In [Ravichandra (2004)], Eq. 3 and 11, respectively, are used to compute wear rates for multi-size particulate flow (with six size classes) in a pipe. The test cases correspond to the experiments of [Gupta, Singh, Seshadri (1995)], the details of which are presented in Tab. 1. The material of the wear specimen used in [Gupta, Singh, Seshadri (1995)] was mild steel with specific energy coefficients for impact and sliding wear for mild steel [Ravichandra (2004)]. In pipe flow, the angle of impact is usually very small and hence the impact wear coefficient $E_I(\alpha)$ may be assumed constant with respect to α. The value E_I in Tab. 1 is this constant value. Note that the specific energy of impact, E_I, is two orders of magnitude higher than the specific energy of sliding wear, E_{SP}.

Table 1: Details of cases used in comparison of predicted wear rates of [Ravichandra (2004)] with experimental results of [Gupta, Singh, Seshadri (1995)]

Case	D (mm)	$d_p(\mu$m)	$\%C_{avg}$	$\%C$ of each Species	W_m (m/s)	E_{sp}(J/m^3)	E_I(J/m^3)
W1	55	438, 235, 168, 127, 91, 38	10.8	0.82, 1.44, 0.74, 2.50, 1.63, 3.67	1.95	1.56E11	1.56E13
W2	55	438, 235, 168, 127, 91, 38	10.8	0.82, 1.44, 0.74, 2.50, 1.63, 3.67	2.75	1.56E11	1.56E13

In Fig. 2 (reproduced with permission), predicted normalized wear rates [Ravichandra (2004)] are compared with the experimental wear results of [Gupta, Singh, Seshadri (1995)] for a mild steel pipe (Case W1 and W2 of Tab. 1). The maximum and average difference between prediction [Ravichandra (2004)] and experiment [Gupta, Singh, Seshadri (1995)] are 24% and 10%, respectively. The discrepancy in the results is attributed by [Ravichandra (2004)] to attrition (particle break-up) in closed loop systems, and possible sources of error due to particle sampling and size measurement. An extra source of error is in the use of particle-size independent E_I and E_{SP} values. However, the trends in the predicted normalized wear rates of [Ravichandra (2004)] agree reasonably closely with the experimental results of [Gupta, Singh, Seshadri (1995)] under similar operation conditions. In the absence of experimental data for wear in rotating channels, this favorable comparison in case of pipes gives confidence in applying the methodology to the present problem.

5 Results of erosion wear in rotating channel

Erosion wear is a complex boundary phenomenon and is greatly affected due to the local flow conditions in the vicinity of the wall, particularly the solids velocity and concentration distributions adjacent to the channel walls. In order to gain a qualitative insight into erosion wear trends from the computed multi-size particulate

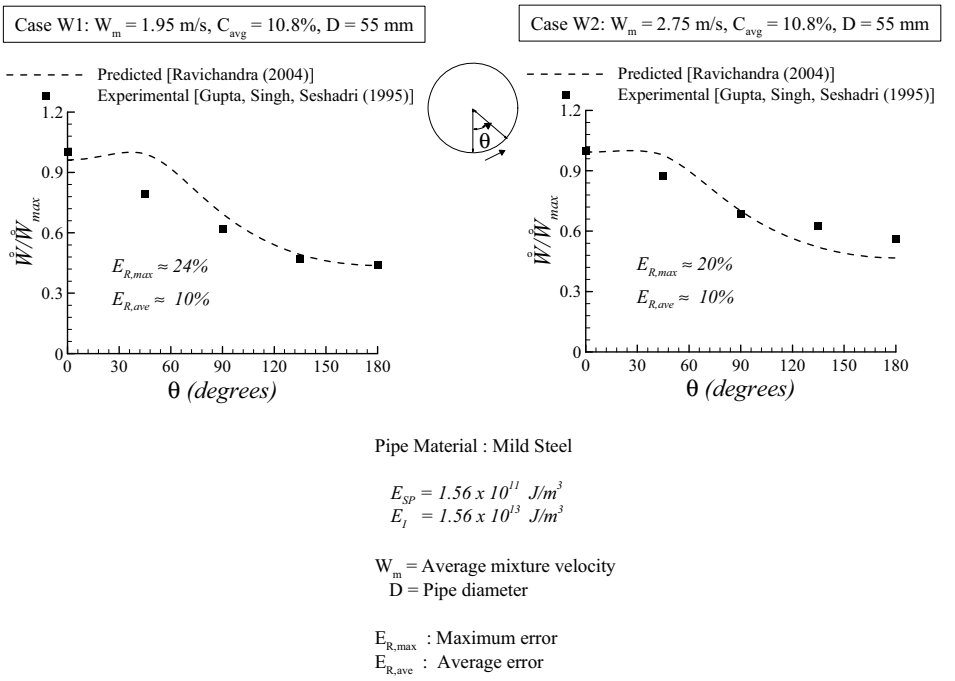

Figure 2: Reproduced plot from [Ravichandra (2004)] showing comparison between predicted normalized wear rates [Ravichandra (2004)] with experiments of [Gupta, Singh and Seshadri (1995)] (Case W1 and W2 of Tab. 1)

flow field, results relevant to erosion wear prediction are presented (using a single representative case) in this section in brief.

With respect to the flow conditions along the walls, the salient features of the results discussed elsewhere [Gupta and Pagalthivarthi (2007), Gupta and Pagalthivarthi (2006a), Gupta and Pagalthivarthi (2006b)] are revisited as follows.

With increase in the height-based rotation number Ro_H (keeping Reynolds number constant), inlet (average) concentration, C_{avg}, and bulk flow Reynolds number, Re_H (keeping rotation number constant), the concentration (overall and species) shows an increasing trend in x-direction along the channel pressure side (PS) and decreasing trend along the channel suction side (SS).

At $Ro_H \ll 0.04$, mixture velocity decreases initially with x along channel pressure side and saturates. Whereas, at the suction side, the mixture velocity continues to decrease at all rotation numbers. At $Ro_H > 0.04$, however, after an initial decrease up to a third of channel length, the mixture velocity shows an increase along the

pressure side due to the centrifugal effect. This phenomenon is also exhibited by the mixture velocity at higher average concentrations and flow Reynolds number (keeping rotation number constant).

Since particles reasonably closely follow the mixture in the stream-wise direction, it is found that velocity of the solids species also behaves in a manner similar to mixture velocity (as stated in the second point).

The y-component of solids velocity, v_k, shows particle size dependence – its magnitude is larger for larger particle sizes. Moreover, the magnitude of v_k is seen to increase under the action of Coriolis force.

These features of particulate flow adjacent to the channel walls are illustrated in Fig. 3. The variation of x-component of solid velocity (u_k), y-component of solid velocity (v_k), and concentration (C_k) along channel walls at $Ro_H = 0.02$ and $Ro_H = 0.12$ are shown for the largest particle size class of slurry A1 (see Case W3 of Tab. 2). The other particles tend to follow similar trends albeit with lower magnitudes of v_k. (Note: In Tab. 2, d_w, H, and L, respectively, are the weighted-mean diameter of slurry, channel height, and length.)

The sliding wear rate is a function of the wall shear stress and tangential velocity (u_k) and concentration of the solids species. At lower rotation numbers $(Ro_H < 0.04)$, the decreasing trend of species velocity (u_k) and increasing trend of particulate concentration along channel pressure side (see Fig. 3a and 3b) could be expected to yield a somewhat flatter sliding wear rate along the pressure side. At higher rotation numbers $(Ro_H > 0.04)$, solid velocity increases after a certain channel length (depending upon the rotation number) while the concentration shows increasing trend (with x) along the channel pressure side. Thus sliding wear rate could be expected to increase in effect along the pressure side at higher rotation numbers. However, the decreasing trends in both solids velocity and concentration along channel suction side are expected to result in a decreasing sliding wear rate on the suction side at all rotation numbers.

Impact wear rate on the other hand depends strongly on solids concentration, C_k, the magnitude of velocity, $(V_k = \sqrt{u_k^2 + v_k^2})$ and the angle of impact $\left[\alpha = \tan^{-1}\left(|v_k|/|u_k|\right)\right]$. Along the channel pressure side, there is a sharp increase in $|v_k|$ right near the inlet (under the action of Coriolis force). It is to be noted that v_k is one-two orders of magnitude smaller than u_k. Thus in the computation of impact wear rate using Eq. 8, the impact flux, $C_k V_k^3$, is expected to be dominated by the trends (or magnitude) of u_k along the channel walls. Hence, along the pressure side, impact wear rate could be expected to increase with x at higher rotation numbers $(Ro_H > 0.04)$. Because the velocity v_k is negative, the suction side wall is unlikely to experience impact wear. Thus, in all subsequent discussions, impact wear is restricted to the

pressure side.

To complete the picture, Fig. 4 shows the variation of sliding friction power $\sum_{k=2}^{N+1} \tau_k C_k u_k$ and the factor $\sum_{k=2}^{N+1} C_k V_k^3$ (ρ_k being constant is not included) which appears in the impact wear rate equation, along the channel pressure and suction sides at $Ro_H = 0.02$ and $Ro_H = 0.12$ for Case W3 of Tab. 2. From the trends of friction power and impact flux observed in Fig. 4, the wear rate distributions due to sliding and impact could be qualitatively visualized.

Table 2: List of cases run for parametric studies on wear rate

Case	H/L	$d_p(\mu\text{m})$	$\%C_{avg}$	C_k % age of C_{avg}	d_w (μm)	Re_H	Ro_H	E_{I0} (J/m^3)
W3 (Slurry A1)	0.05	750, 500, 250, 150, 100, 50	8, 12, 18	5, 10, 15, 15, 25, 30	187.5	1.75E5	0.02, 0.04, 0.06, 0.08, 0.10, 0.12	2.77E15
W4 (Slurry A2)	0.05	750, 500, 250, 150, 100, 50	12	20, 20, 20, 15, 15, 10	342.5	1.75E5	0.04, 0.08, 0.12	2.77E15
W5 (Slurry B1)	0.05	900, 700, 400, 200, 125, 40	12	10, 15, 15, 15, 20, 25	320	1.75E5	0.04, 0.08, 0.12	2.77E15
W6 (Slurry B2)	0.05	900, 700, 400, 200, 125, 40	12	16.67, 16.67, 16,67, 16.67, 16.67, 16.67	394.5	1.75E5	0.04, 0.08, 0.12	2.77E15
W7 (Slurry C1)	0.05	738, 255, 180, 128, 91, 38	12	5, 10, 20, 40, 10, 5	167.5	1.75E5	0.04, 0.08, 0.12	2.77E15
W8 (Slurry C2)	0.05	738, 255, 180, 128, 91, 38	12	5, 15, 30, 30, 10, 10	180.	1.75E5	0.04, 0.08, 0.12	2.77E15
W9	0.05	750, 500, 250, 150, 100, 50	12	5, 10, 15, 15, 25, 30	187.5	1.75E5, 2.5E5, 3.5E5, 5E5	0.04	2.77E15
W10	0.05	750, 500, 250, 150, 100, 50	12	5, 10, 15, 15, 25, 30	187.5	1.75E5, 2.5E5, 3.5E5, 5E5	0.08	2.77E15
W11	0.05	750, 500, 250, 150, 100, 50	12	5, 10, 15, 15, 25, 30	187.5	1.75E5, 2.5E5, 3.5E5, 5E5	0.12	2.77E15

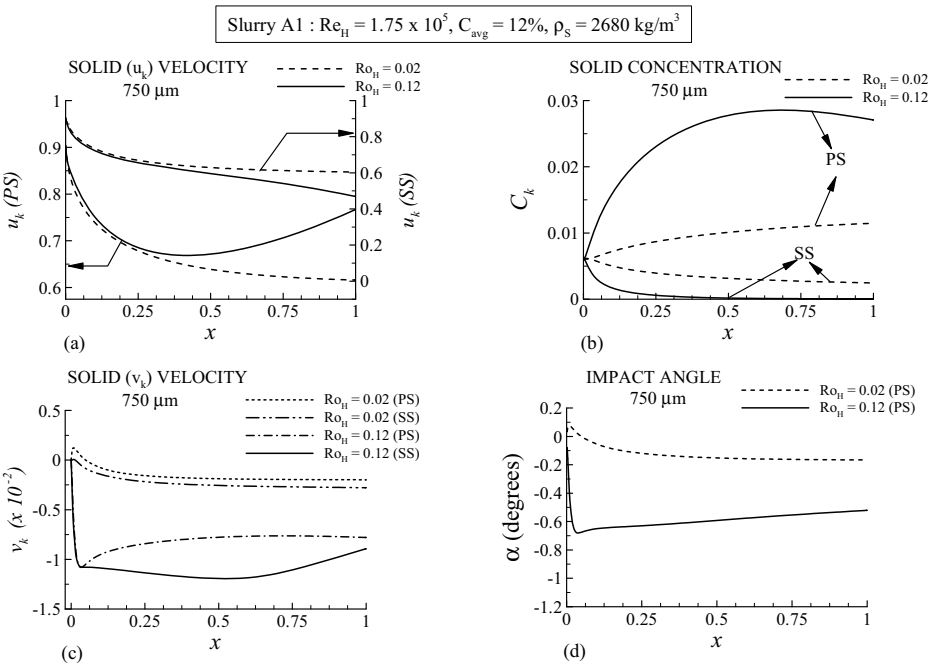

Figure 3: Variation of (a) solid u-velocity, (b) solid concentration, (c) solid v-velocity and (d) impact angle along the channel PS and SS for the largest particle size (750 microns) (Case W3 of Tab. 2)

6 Wear rates in multi-size particulate flow through rotating channel

In this section, important results that bring out the effect of operating parameters on erosion wear rate are discussed. The compositions of slurries and the range of various governing parameters are listed in Tab. 2. In all the cases, the density of all six size classes is 2680 kg/m^3. In general, both sliding and impact wear rates are computed using the particle size-dependent specific energy coefficients in the wear models (Eq. 8 and 15, respectively). However, in Fig. 5 (a-b), a quick comparison of the wear rates predicted by using d_p-dependent E_{sp} and those predicted by using E_{sp} corresponding to d_w (the weighted diameter) are presented. Trends of both sets of results are similar for this operating condition. Similar trends are observed for comparison of pressure side impact wear rates (Fig. 5(c)) predicted by using d_p-dependent E_I and those predicted using E_I corresponding to d_w. The main point to note is that the difference would in general be a function of the PSD and other parameters.

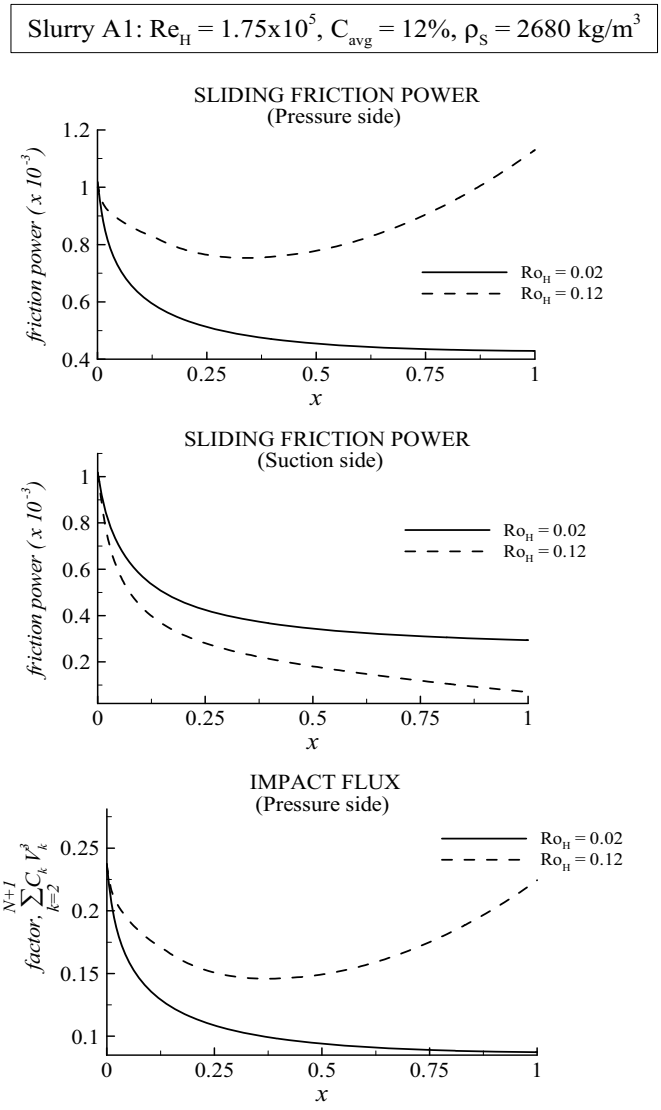

Figure 4: Sliding friction power (along PS and SS) and impact flux factor along channel PS at $Ro_H = 0.02$ and $Ro_H = 0.12$ (Case W3 of Tab. 2)

6.1 Effect of rotation number

The effect of rotation number is shown in Fig. 6 for Case W3 of Tab. 2 (for slurry A1 with $Re_H = 1.75 \times 10^5$, $C_{avg} = 12\%$). As stated previously impact wear rate is shown only on the pressure side.

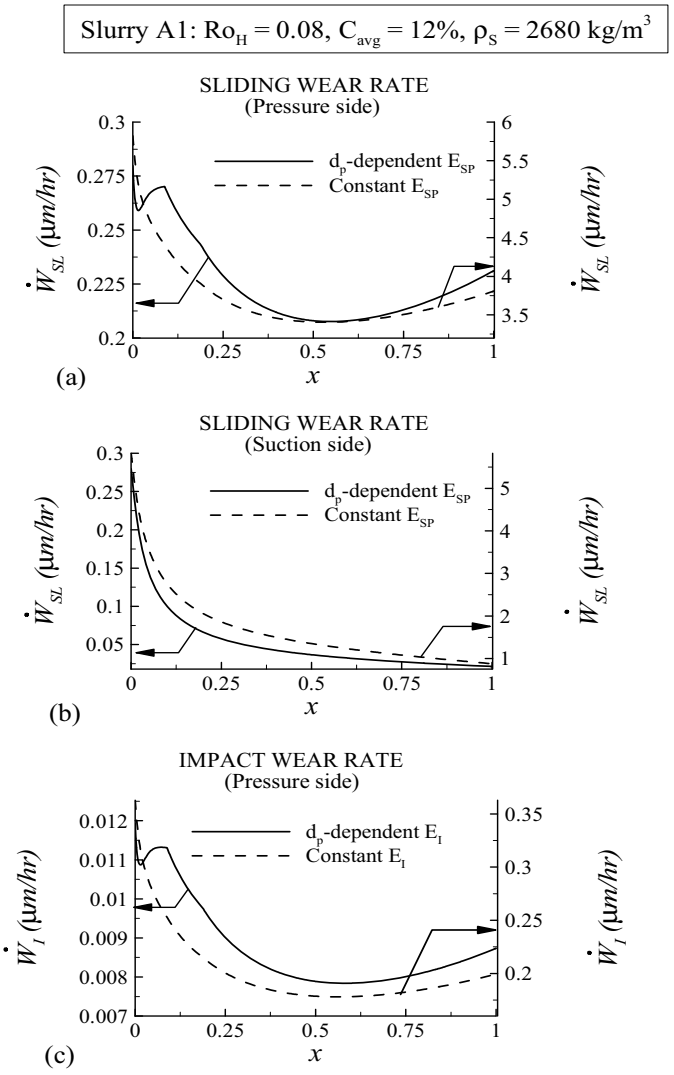

Figure 5: Sliding and impact wear rates along PS and SS for constant and particle-size dependent energy coefficients (Case W3 of Tab. 2)

The wear coefficients used are for the combination of sand particles and white iron alloy wear material. The particle size dependence of the wear coefficients is according to the Eq. 5 and 13.

The following general observations may be made from Fig. 6:

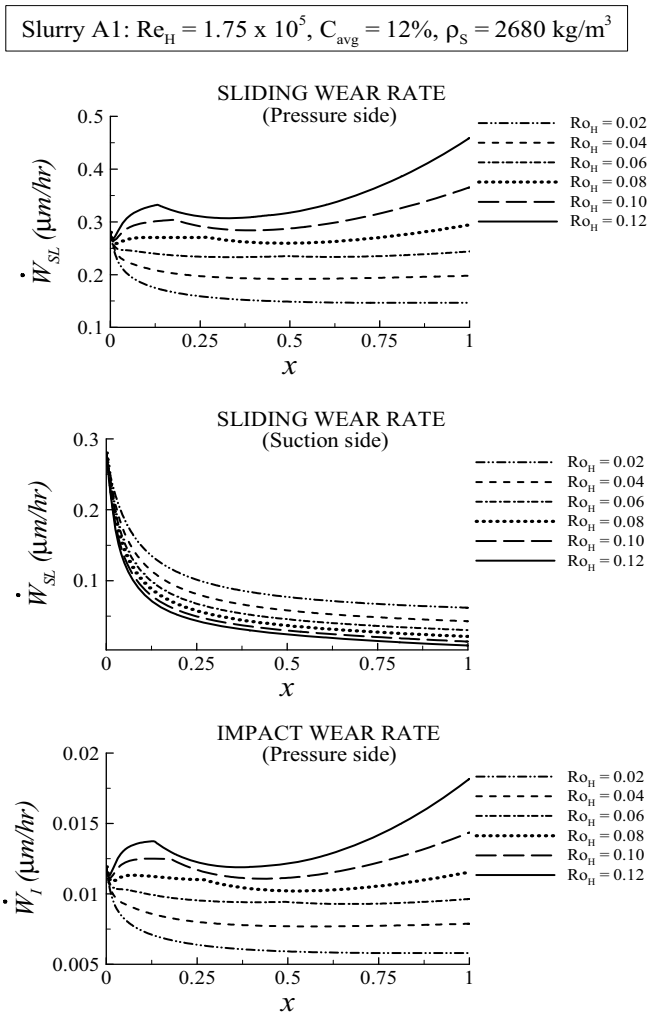

Figure 6: Sliding wear rates along PS (top) and SS (middle) and impact wear rate on the PS (bottom) for different values of rotation numbers (Case W3 of Tab. 2)

The impact wear rate is typically much smaller than sliding wear rate for all Ro_H (0.02 to 0.12).

On the suction side sliding wear rate decreases with increasing rotation number. Right at the inlet the shear stress is high because the entrance velocity (U_0) must quickly decelerate to satisfy the law of the wall. The shear stress begins to drop quickly with increasing x. Likewise the tangential velocity (u_k) also decreases. The

overall effect is that for a given Ro_H, the wear rate (proportional to $\tau_k u_k$) decreases with x.

On the pressure side similar trend is seen at $Ro_H = 0.02$, although the wear rate (even at $Ro_H = 0.02$) is higher on the pressure side than on the suction side. This is due to the slightly higher velocity at the pressure side wall (see Fig. 3(a), for example). As Ro_H increases, the wear rate increases. However, for $Ro_H > 0.06$, the pressure side wear rate trend is considerably different from the suction side wear rate distribution. At $Ro_H = 0.02$ and 0.12, for example, a local peak is seen near the entrance. After a subsequent drop, the wear rate again continues to increase. This is simply a reflection of the variation in u_k near the wall (see Fig. 3(a)), and the concentration C_k (Fig. 3(b)).

The impact wear rate shows a similar trend as the sliding wear rate on the pressure side. Recall that impact wear rate depends on $\sum \rho_k C_k V_k^3$, with $V_k^2 = \left(u_k^2 + v_k^2\right)$. Since $v_k << u_k$, $V_k^2 \sim u_k^2$ and hence the impact wear rate basically varies as $\rho_k C_k u_k^3$. The sliding wear rate on the other hand depends on $C_k u_k \tau_k \ \left(C_k u_k u_{\tau k}^2\right)$ which again varies as $\sim C_k \rho_k u_k^3$. The difference in the wear rates due to sliding and impact wear rate is due to the difference in the respective wear coefficients.

6.2 Effect of particle size distribution

The sliding and the impact wear rates distribution depends on the particle size distribution. Fig. 7-9 depict this for six particle size distributions (Cases W3-W8 of Tab. 2) at three rotation numbers ($Ro_H = 0.04, 0.08$ and 0.12).

Slurries A1, C1 and C2 all have weighted average diameters of 187.5, 167.5 and 180 μm, which are quite close to each other, respectively. However, the proportions of constituent particle sizes are different. The following observations may be made from Fig. 7 – 9:

In a broad sense, the larger the d_w, the larger is the wear rate.

For slurries with approximately equal d_w (for example A1, C1 and C2), the predicted wear rates are nearly equal. However, Slurry A1 is small particle dominated, C1 is dominated by particles of intermediate size, and Slurry C2 is similar to C1 (except that it has more fines than C1). Fig. 7-9 show that the sliding wear rate (both pressure and suction sides) and the impact wear rate are slightly higher for Slurry A1 at all the three Ro_H values. Similarly, Slurry B2 with the largest d_w $(394.5\,\mu m)$ has the maximum wear rate.

As seen in Fig. 7 and 9, at larger Ro_H, all slurries exhibit larger wear rates in general. At $Ro_H = 0.08$, and $Ro_H = 0.1$ the wear rate curves show the typical hump (or peak) near the entrance, followed by a drop to a local minimum, and again increasing.

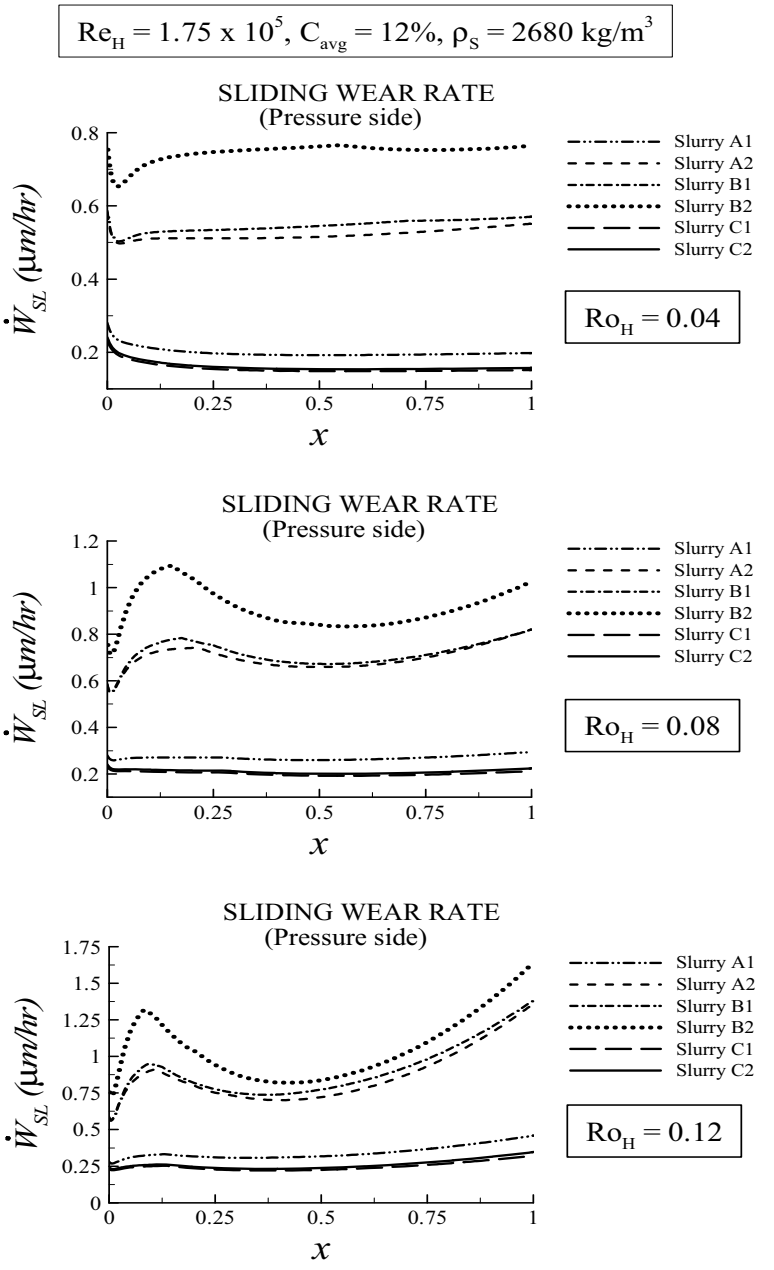

Figure 7: Sliding wear rates along the PS for different slurries at $Ro_H = 0.04$ (top), $Ro_H = 0.08$ (center) and $Ro_H = 0.12$ (bottom) (Cases W3-W8 of Tab. 2).

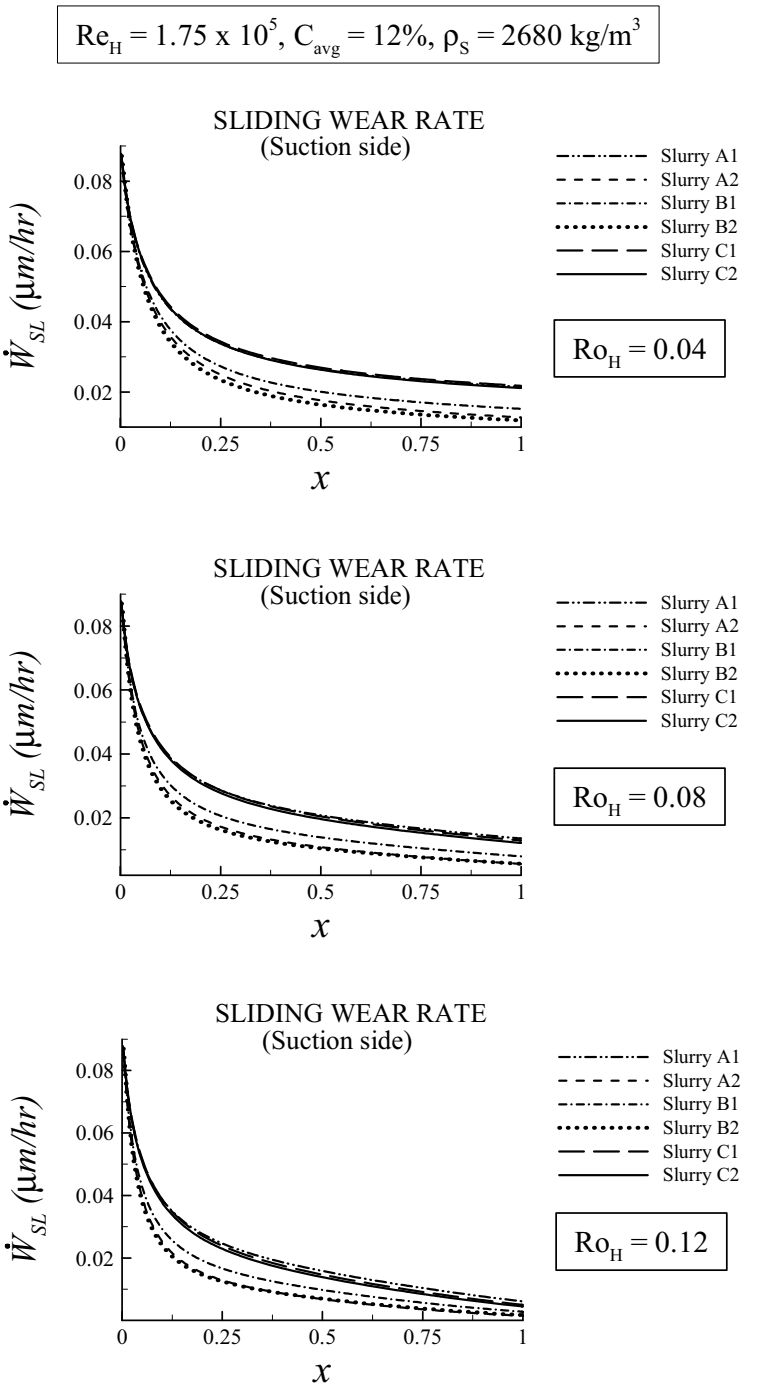

Figure 8: Sliding wear rates along the SS for different slurries at $Ro_H = 0.04$ (top), $Ro_H = 0.08$ (center) and $Ro_H = 0.12$ (bottom) (Cases W3-W8 of Tab. 2).

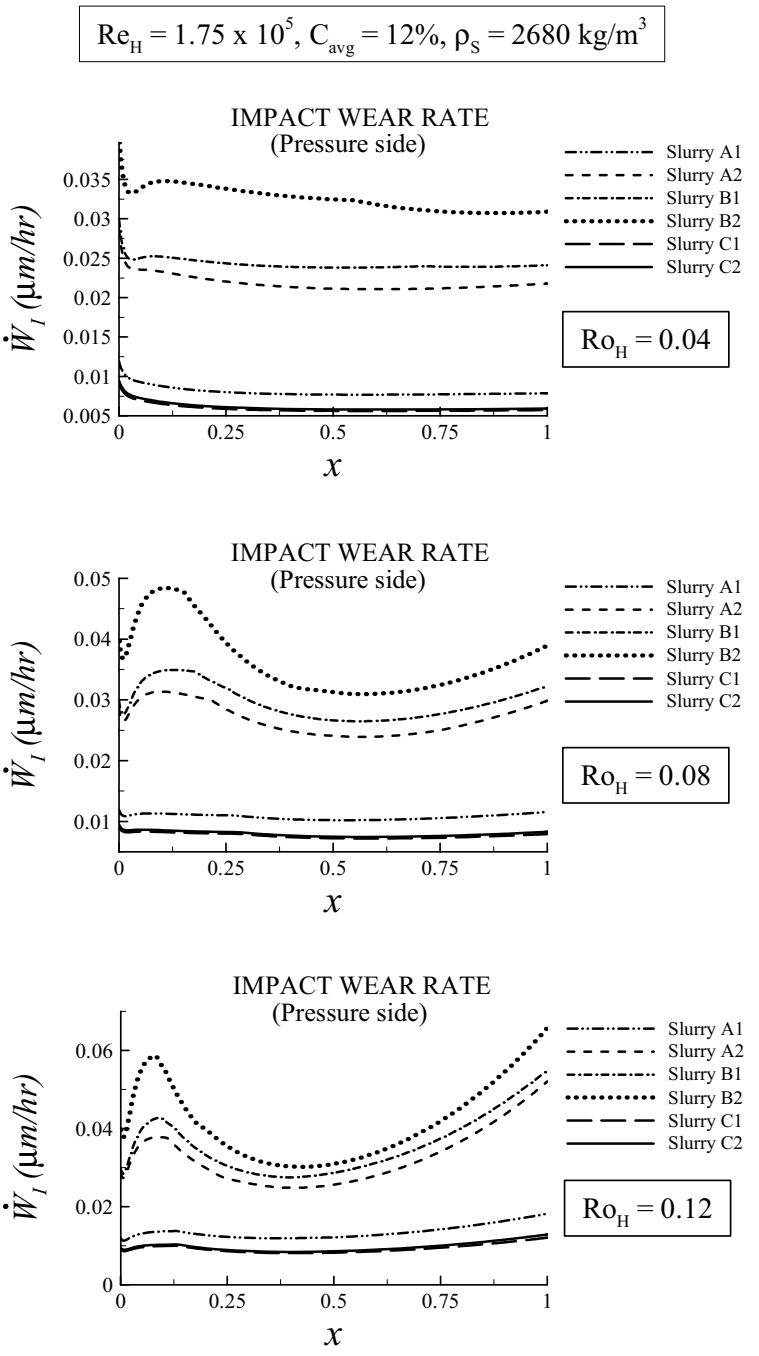

Figure 9: Impact wear rates along the PS for different slurries at $Ro_H = 0.04$ (top), $Ro_H = 0.08$ (center) and $Ro_H = 0.12$ (bottom) (Cases W3-W8 of Tab. 2).

On the suction side, sliding wear rate is initially relatively large. The wear rate decreases significantly as d_w increases. After a drastic decrease with increasing x, wear rate falls off to nearly zero. This is explained as follows. Near the entrance, the slurry concentration is nearly equal to the entrance value. Moreover, as discussed previously, the wall shear stress is considerably high. On the top of this as d_w increases, the effective E_{sp} decreases. All the three factors contribute to the relatively high wear rate near $x = 0$ on the suction side. Now as x increases, particles tend to migrate towards the pressure side, especially the largest particles. In addition, there is also a decline in the shear stress as well as u_k. All these factors contribute to the drastic reduction in $\dot{W}_{SL}$ to nearly zero value at the channel exit on the suction side.

Again it is seen that impact wear rate is significantly less than the corresponding sliding wear rates on the pressure side.

6.3 Effect of inlet concentration

Fig. 10 and 11 show the effect of varying inlet concentration on the sliding and impact wear rates for Case W3 of Tab. 2 with $Ro_H = 0.04$ and $Ro_H = 0.1$. The following observations may be made with reference to these figures.

Both impact wear rate and sliding wear rate increase with increasing C_{avg}. As the concentration C_{avg} increases, so does $C_k$along the walls and hence the wear rate as well.

For the larger rotation number of $Ro_H = 0.1$, the wear rate on the pressure side increases, while the wear rate on the suction side decreases. This is because with the increased Coriolis force, the particles tend to concentrate near the pressure side, thus resulting in greater wear.

With increased Ro_H, the peak in the wear rate near the entrance of the channel disappears as C_{avg} increases.

6.4 Effect of bulk flow Reynolds number

The effect of bulk Reynolds number (Re_H) is shown in Fig. 12-14 for Cases W9-W11 of Tab. 2. The inlet concentration is 12% (C_{avg}). Note that for a fixed channel geometry and fluid, an increase in Re_H at fixed Ro_H increases both U_o and Ω, the rotating speed of the channel. Thus the Coriolis force $(2\Omega m_p U_o)$ (m_p being the particle mass) increases significantly (for increase in Re_H, Ro_H =constant). For example, as Re_H increases from 1.75×10^5 to 5×10^5, U_o increases from 3.5 m/s to 10 m/s. To keep Ro_H fixed at 0.08, Ω must increase by a factor of $(10/3.5 \cong 2.857)$ as well, so that the Coriolis force on the given particle increases by a factor of more than 8. This results in a substantial increase in the Coriolis force on the particles.

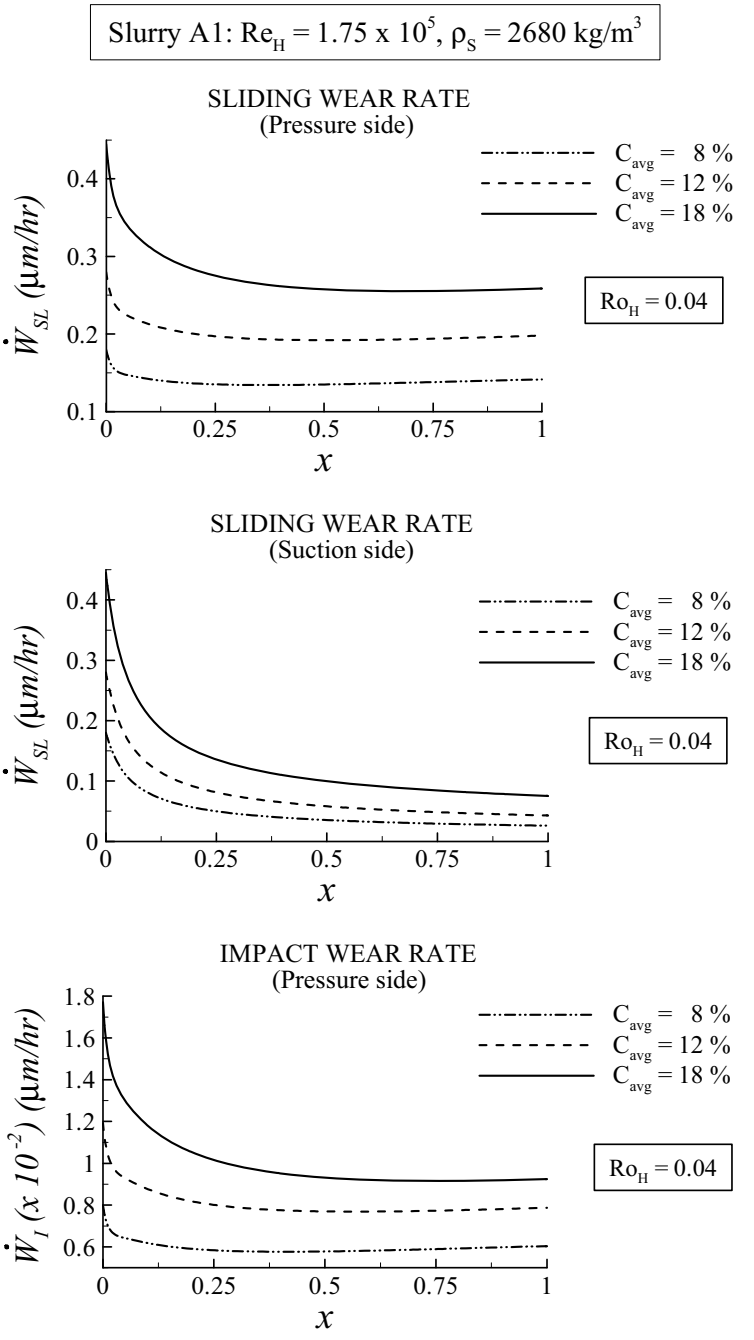

Figure 10: Sliding wear rates along PS (top), SS (middle) and impact wear rates along PS (bottom) for different inlet (average) concentrations at $Ro_H = 0.04$ (Case W3 of Tab. 2)

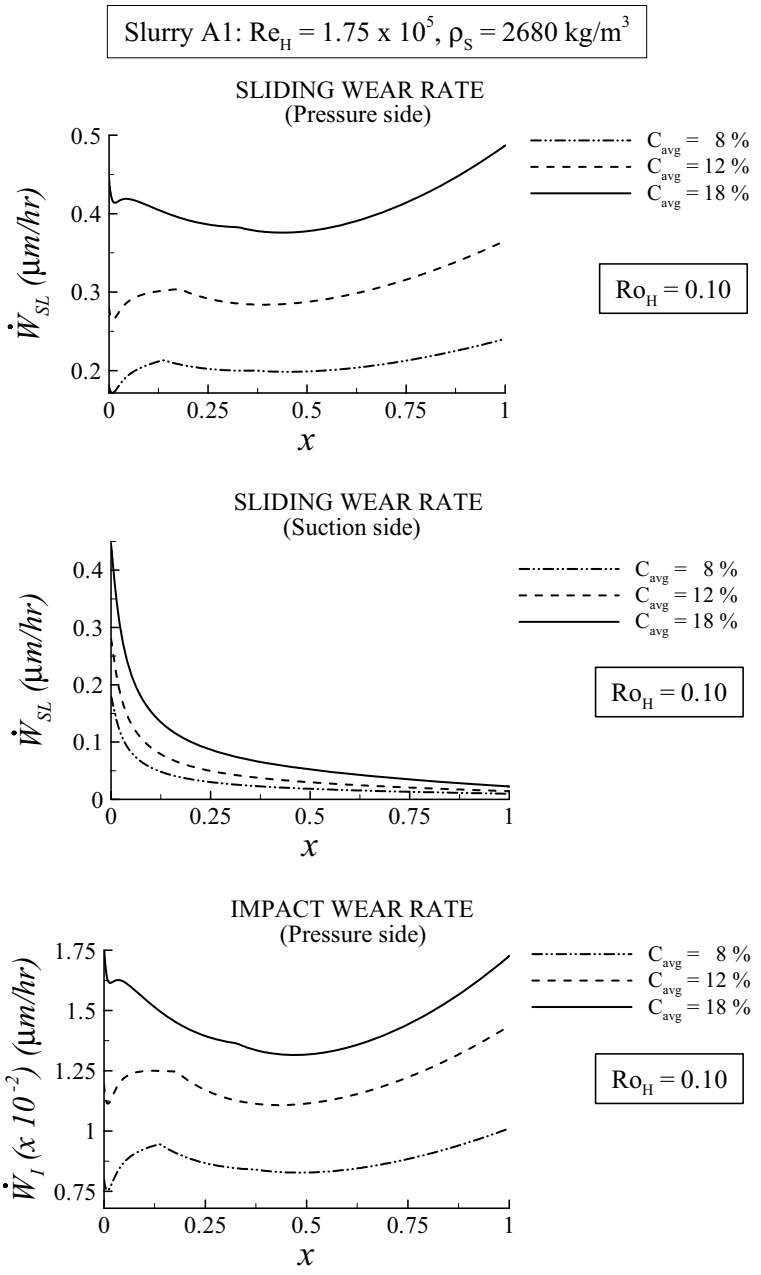

Figure 11: Sliding wear rates along PS (top), SS (middle) and impact wear rates along PS (bottom) for different inlet (average) concentrations at $Ro_H = 0.1$ (Case W3 of Tab. 2)

The following observations are made with reference to Fig. 12-14.

As Re_H increases at fixed Ro_H, the sliding and impact wear rates increase. This is due to the increased velocity as well as the increased concentration along the pressure side. On the suction side, although there is an increase in the velocity (with increase in Re_H), the concentration $C_k$actually decreases. Hence the increase in wear rate on the suction side with increasing Re_H is less pronounced than on the pressure side.

At a fixed Re_H (say 5×10^5), an increase in Ro_H causes similar effects to those shown in Fig. 12. The characteristic hump (or peak) occurs for $Ro_H \geq 0.08$ as shown in Fig. 13 and 14.

It is again noted that impact wear rates are much lesser than sliding wear rates.

Thus, from the various results reported in this section, the complex relation between wear rate and rotational speed, inlet concentration, inlet velocity and PSD are clearly seen.

7 Conclusions

Dense slurry flow through rotating channel has been numerically investigated using finite element methodology. The flow field thus obtained is used to relate the local velocity and concentration near the channel walls to wear rate *via* suitable wear models. Wear models have been modeled as a function of the local flow conditions and particle size-dependent wear coefficients (obtained from the open literature) for the chosen slurry/material combination (sand slurry and white iron alloy material). The following conclusions are drawn from the present study:

Sliding wear rate is observed to be 10-50 times higher compared to the impact wear rates in rotating channel flow for the range of parameters used in this study.

The effect of different operating parameters on the local flow conditions (and hence wears rates) is quite complex. The general trends observed are that the maximum wear rate usually occurs either at the inlet or at the exit subject to the operating parameters. With increase in rotation speed, the local solids concentration will increase at the pressure side causing an increase in the wear rate on the pressure side and a corresponding decrease on the suction side. An increase in the bulk Reynolds number and the average inlet concentration also produce similar effect on the wear rates.

A significant contribution to the sliding wear rate comes from slurries having larger weighted mean diameters.

An important conclusion relevant to the present study is that wear rate prediction using a single representative diameter (like D50 diameter) may be seriously in error,

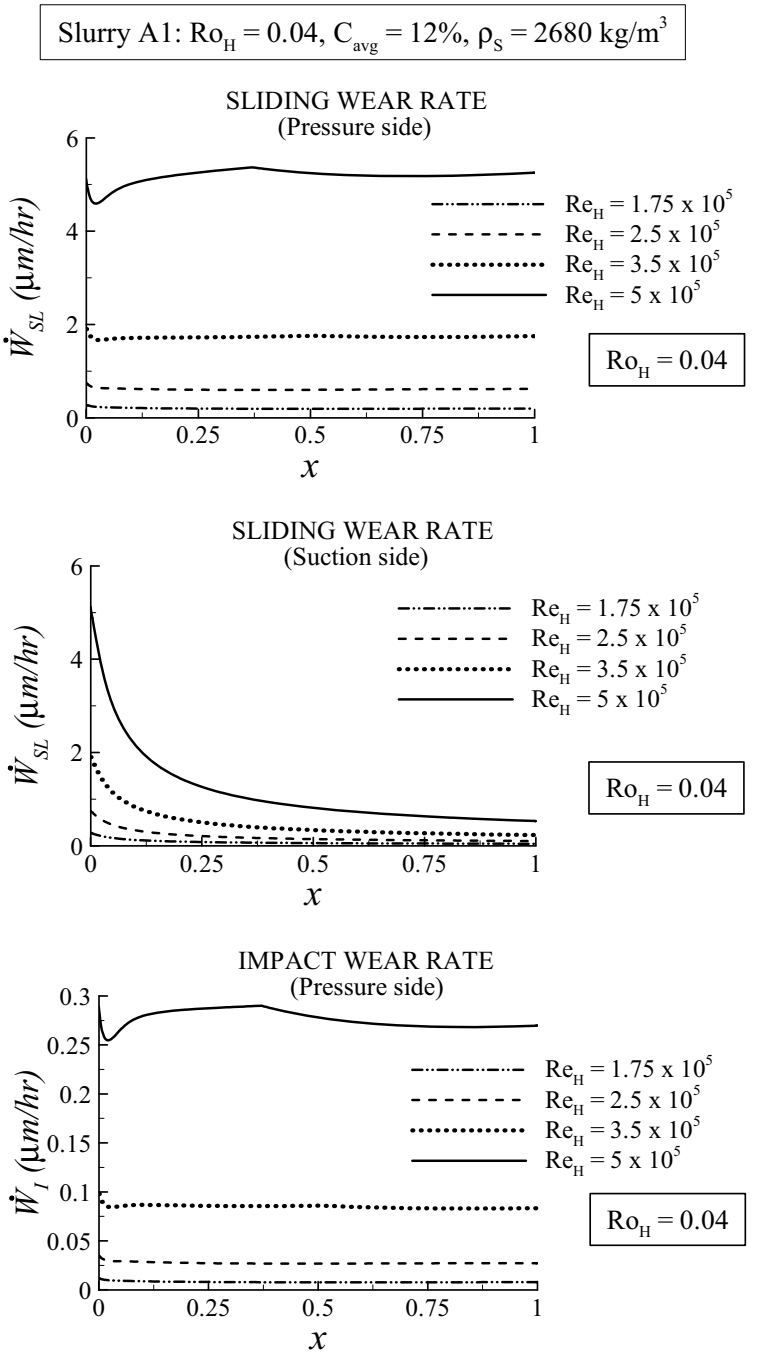

Figure 12: Sliding wear rates along PS (top), SS (middle) and impact wear rates along PS (bottom) for different Re_H at $Ro_H = 0.04$ (Cases W9-W11 of Tab. 2)

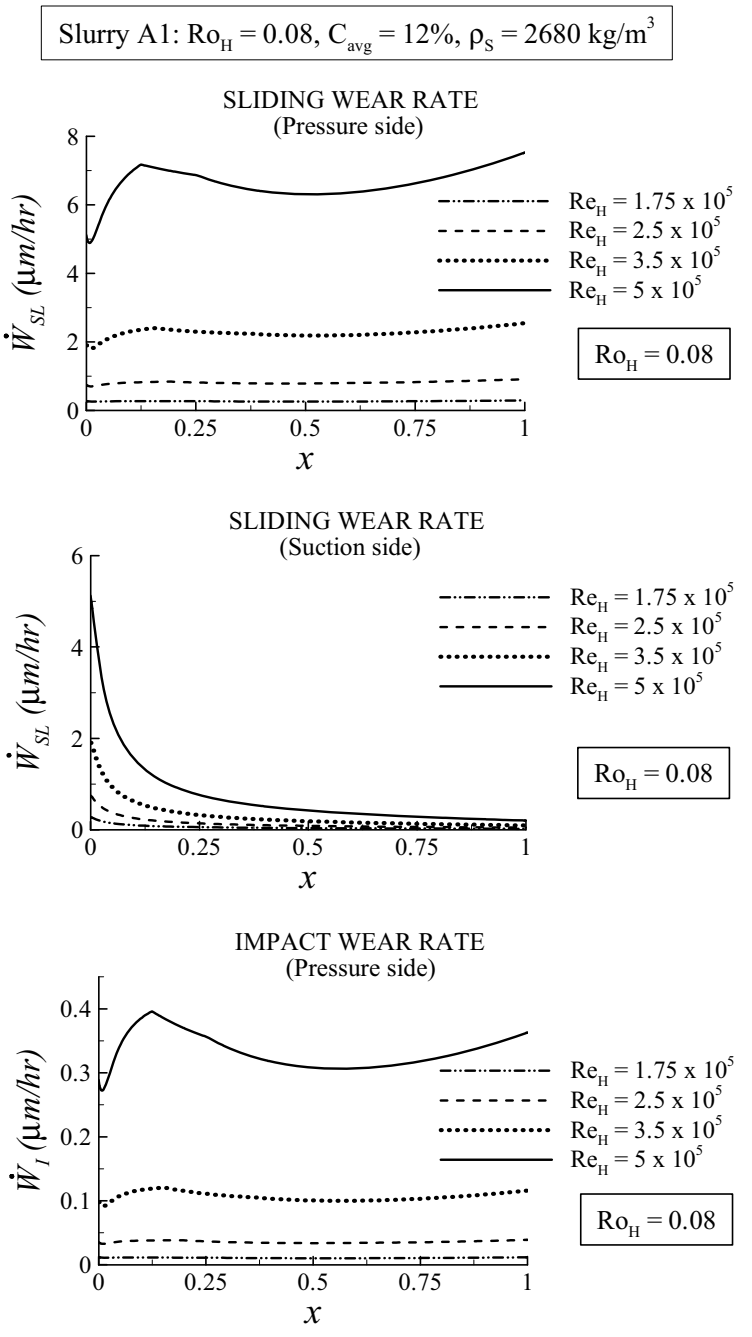

Figure 13: Sliding wear rates along PS (top), SS (middle) and impact wear rates along PS (bottom) for different Re_H at $Ro_H = 0.08$ (Cases W9-W11 of Tab. 2)

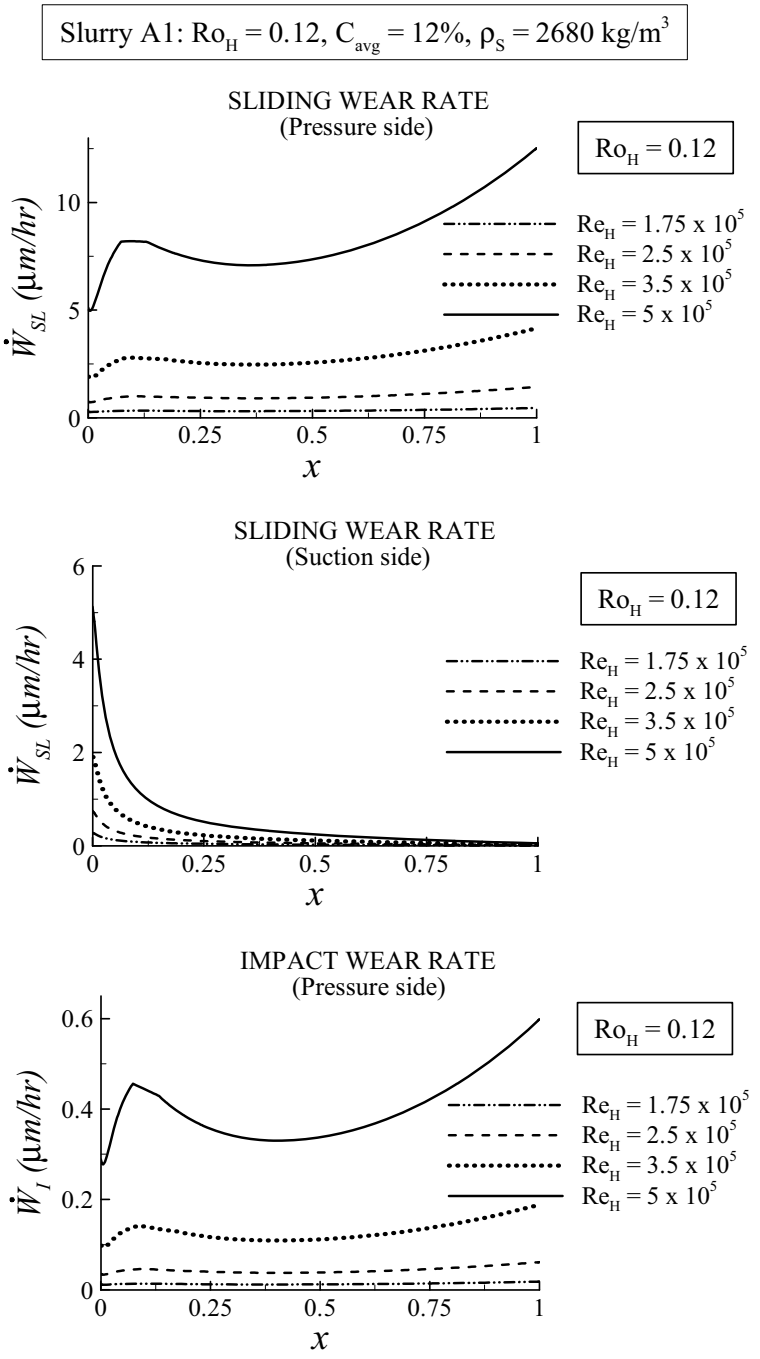

Figure 14: Sliding wear rates along PS (top), SS (middle) and impact wear rates along PS (bottom) for different Re_H at $Ro_H = 0.12$ (Cases W9-W11 of Tab. 2)

especially if the particle size distribution is broad. In such cases, accurate wear prediction could be obtained by characterizing the particle size distribution into suitable number of size classes, and accounting for the particle-size dependence in the wear model(s). Based on the predictions for several slurries with various PSDs, suitable correlations can be developed for an "equivalent particle size" which would yield the same wear rate as that obtained for the actual particle size distribution. Such an "equivalent particle size" could be useful in treating the slurry as consisting of mono-size particles in designing for erosion wear.

References

Addie, G. R.; Sellgren, A.; Mudge, J. (2001): SAG mill pumping cost considerations. SAG Conference, *3rd International Conference on Autogenous & Semiautogenous Grinding Technology*, September 30 – October 3, 2001, Vancouver, B.C., Canada.

Addie, G. R.; Sellgren, A. (1998): Effect of wear on the performance of centrifugal slurry pumps. *ASME Fluids Engineering Summer Meeting*, Washington, D.C.

Addie, G.R.; Pagalthivarthi, K.V. (1989): Prediction of dredge pump shell wear. In: *Proceedings of the WODCON XII, 12th World Dredging Conference*, World Organization of Dredging Associations, Arlington, VA, 1989, pp. 481-504.

Clark, H. McI.; Tuzson, J.; Kien, K. Wong. (2000): Measurements of specific energies for erosive wear using Coriolis erosion tester. *Wear*, Vol. 241, pp. 1-9.

Gupta, P.K.; Pagalthivarthi, K.V. (2006a): Effect of inlet concentration on solid-liquid mixture flow through rotating channel. In *Proceedings of International Congress on Computational Mechanics and Simulation* – 2006, December 8-10, 2006, IIT Guwahati, India.

Gupta, P.K.; Pagalthivarthi, K.V. (2006b): Effect of particle size distribution on multi-size particulate flow through rotating channel. In *Proceedings of NCFMFP 33rd National and 3rd International Conference on Fluid Mechanics and Fluid Power*, December 7-9, 2006, IIT Bombay, India.

Gupta, P.K.; Pagalthivarthi, K.V. (2007): Finite element prediction and validation of multi-size particulate flow in rotating channels. *Progress in Computational Fluid Dynamics – An International Journal*, Vol. 7, No. 5, pp. 247-260.

Gupta, R.; Singh, S.N.; Seshadri, V. (1995): A study on the uneven wear rate in a slurry pipeline. *Bulk Solids Handling*, Vol. 15, No. 4, pp. 603-607.

Kaushal, D.R., Seshadri, V.; Singh, S.N. (2002): Prediction of concentration and particle size distribution in the flow of multi-sized particulate slurry through rectangular duct. *Appl. Math. Model.,* Vol. 26, No. 10, pp. 941-952.

Kaushal, D.R.; Tomito, Y. (2003): Comparative study of pressure drop in multi-sized particulate slurry flow through pipe and rectangular duct. *Int. J. of Multiphase Flow*, Vol. 29, No. 10, pp. 1473-1487.

Pagalthivarthi, K.V.; Helmly, F.W. (1992): Applications of material wear testing to solids transport via centrifugal slurry pumps. *Wear Testing of Advanced Materials, ASTM, STP* 1167, eds. Divakar, R. and Blau, P.J., pp. 114-126.

Pagalthivarthi, K.V.; Veeraraghavan, R. (1998): Numerical insight into experimental results of particle size effect in Coriolis wear tester. *Proc. of the First International FMFP Conference, 15-17 Dec., 1998*, IIT Delhi, New Delhi.

Pagalthivarthi, K. V.; Addie, G. R. (2001): Prediction methodology for two-phase flow and erosion wear in slurry impellers. *4th International Conference on Multiphase Flow*, ICMF-2001, New Orleans, LA, May 27-June 1, 2001.

Ravichandra, J.S. (2004): Numerical study of multi-size particulate flow in horizontal rectangular ducts and pipes. Ph.D. Thesis, Indian Institute of Technology Delhi, India.

Ravichandra, J.S.; Pagalthivarthi, K.V.; Sanghi, S. (2005): Multi-size particulate flow in horizontal ducts – modeling and validation. *Progress in Computational Fluid Dynamics*, Vol. 5, Issue 8, pp. 466-481.

Roco, M.C.; Addie, G.R. (1983): Analytical model and experimental study on slurry flow and erosion in pump casings. *STA*, Vol. 8, pp.263.

Roco, M.C.; Addie, G.R.; Visintainer, R.; Ray, E.L. (1986): Optimum wearing high efficiency design of phosphate slurry pumps. *Proc. 11th Int. Conf. On Slurry Technology*, Slurry Transport Assoc., Washington, DC, pp. 277-285.

Roco, M. C.; Cader T. (1988): Numerical method to predict wear distribution in slurry pipelines. In: G. Jones, J. Thorn (Eds.), *Advances in Pipeline Protection*, BHRA, Cranfield, UK.

Roco, M.C.; Nair, P.; Addie, G.R. (1984): Test approach for dense slurry erosion. In: *Slurry Erosion: Uses, Applications, and Test Methods ASTM STP 946*, American Society of Testing and Materials, 1984, pp. 185-210.

Roco, M.C.; Nair, P.; Addie, G.R.; Dennis, J. (1984): Erosion of concentrated slurries in turbulent flow. In: M.C. Roco (Ed.), *Liquid–Solid Flows and Erosion Wear in Industrial Equipment*, vol. 13, ASME-FED, New Orleans, 1984, pp. 69-77.

Tian, H.H.; Addie, G.R.; Pagalthivarthi, K.V. (2005): Determination of wear coefficients for prediction through Coriolis wear testing. *WEAR*, Vol. 259, pp. 160-170.

Tuzson, J.J.; Clark, H. Mcl. (1998) The slurry erosion process in the Coriolis

wear tester. *Proc. FEDSM '98, ASME Fluids Engg., Division Summer Meeting, June 21-25, 1998*, Washington, D.C., paper no. FEDSM98-5144.

Tuzson, J.J.; Scheibe-Powell, K.A. (1984): Slurry erosion tests with centrifugal erosion tester. In: M.C. Roco (Ed.), *Liquid-Solid Flows and Erosion Wear in Industrial Equipment*, Vol. 13, ASME-FED, pp. 84-87.

Visintainer, R.; Pagalthivarthi, K.V.; Tian, H.H. (2005): Wear coefficient's dependence on particle size. GIW Internal Report.